高压物理学报

简论钢板在平头弹撞击下的穿透

杨岚夫 文鹤鸣

A Brief Discussion on the Perforation of Steel Plates Impacted by Flat-Nosed Projectiles

YANG Lanfu, WEN Heming

引用本文:
杨岚夫, 文鹤鸣. 简论钢板在平头弹撞击下的穿透[J]. 高压物理学报, 2025, 39(6):064202. DOI: 10.11858/gywlxb.20240912
YANG Lanfu, WEN Heming. A Brief Discussion on the Perforation of Steel Plates Impacted by Flat-Nosed Projectiles[J]. Chinese Journal of High Pressure Physics, 2025, 39(6):064202. DOI: 10.11858/gywlxb.20240912

在线阅读 View online: https://doi.org/10.11858/gywlxb.20240912

DOI: 10.11858/gywlxb.20240912

A Brief Discussion on the Perforation of Steel Plates Impacted by Flat-Nosed Projectiles

YANG Lanfu, WEN Heming

（*CAS Key Laboratory of Mechanical Behavior and Design of Materials*, *Department of Modern Mechanics*, *University of Science and Technology of China*, *Hefei* 230027, *Anhui*, *China*）

Abstract: A theoretical analysis on the perforation of Weldox 460E steel plates struck by flat-nosed projectiles is presented using a previously developed model within a unified framework. This model contains a dimensionless empirical equation to describe the variation of energy absorbed through global deformation as a function of impact velocity. The study further investigates the energy absorption mechanisms of Weldox 460E steel plates, with particular focus on the “plateau” phenomenon, i. e., limited increase in ballistic limit with increasing plate thickness. This phenomenon is explained and compared with results from previously studied 2024-T351 aluminium plates. The model predictions agree well with experimental data for Weldox 460E steel plates impacted by flat-nosed projectiles, including: relationship between global deformation and impact velocity, ballistic limit, residual velocity, and critical conditions for the transition of failure modes. Moreover, the model effectively predicts the “plateau” phenomenon observed in intermediate plate thickness range. It is also found that the indentation absorption energy contributes a significantly larger fraction of the total absorption energy in Weldox 460E steel plates perforated by flat-nosed projectiles than in 2024-T351 aluminium plates, due to the differences in material properties.

Keywords: theoretical model; flat-nosed projectile; steel plate; perforation; ballistic limit; residual velocity

CLC number: O385; O521.9 **Document code:** A

Steel is widely used in protective structures, and perforation of steel plates by flat-nosed projectiles remains a key topic in penetration mechanics. Extensive research has been conducted through experimental, numerical and theoretical approaches on the perforation behavior of metal plates impacted by blunt projectiles[1−3], with particular focus on steel plates. Over the past few decades, various theoretical models have been developed to describe the perforation process of metal plates by flat-nosed projectiles. These models differ primarily in their assumptions with respect to dominant failure mechanisms, which depend on impact conditions, such as impact velocity, geometries and mechanical properties of both projectile and target plate.

For thin plates impacted by flat-nosed projectiles at low velocities, the plate response is dominated by global deformations, including bending and membrane stretching, accompanied by localized shear plugging or rupture. In such cases, rigid-plastic methods are commonly used to analyze the behavior of both projectiles and targets[4−8]. As plate thickness or impact velocity increases, global deformations diminish and are typically neglected in theoretical analyses, with localized shear plugging becoming the predominant deformation mode. The theoretical

* **Received date:** 2024-10-17; **Revised date:** 2024-12-03

Biography: YANG Lanfu (1998—), male, doctoral student, major in impact dynamics. E-mail: ylf8@mail.ustc.edu.cn

Corresponding author: WEN Heming (1965—), male, Ph.D., professor, major in impact dynamics. E-mail: hmwen@ustc.edu.cn

models addressing this regime generally employ energy balance method[9–10], multi-stage analyses[10–12], and plastic wave theory[13–14]. At high impact velocities and great plate thicknesses, adiabatic shear instability arises during the plugging process of blunt projectiles perforating metal plates, and is the primary focus of theoretical models[15–17].

Børvik *et al*.[18–21] systematically studied the perforation of Weldox 460E steel plates with different thicknesses by flat-nosed projectiles. Their work revealed a distinct "kink" in the ballistic limit-thickness curve, in which the ballistic limit exhibited a slightly increase within intermediate plate thickness range, a characteristic referred to as the "plateau" phenomenon. This behavior was qualitatively attributed to changes in failure mechanism[21]. Recently, Yang *et al*.[22] proposed a theoretical model within a unified framework for metal plate perforation by flat-nosed projectiles. Based on energy absorption analysis, the model accounted for four principal mechanisms: initial inelastic impact, projectile indentation, shear localization, and global deformation. The model introduced a dimensionless empirical equation to describe the relationship between global deformations and impact velocity. The model predictions agreed well with experimental data, including ballistic limit, residual velocity, and critical conditions for the transition of failure modes. Notably, it successfully predicted and explained the "plateau" phenomenon via energy absorption analysis. Further theoretical analysis elucidated how energy absorption components varied with impact velocity and plate thickness. Given its robust predictive capability, this theoretical model is adopted here to analyze the perforation of Weldox 460E steel plates by flat-nosed projectiles.

The objective of this study is to investigate the perforation of Weldox 460E steel plates impacted by rigid flat-nosed projectiles[18–21] using the recently developed theoretical model[22]. Firstly, the dimensionless relationship between global deformation and impact velocity in the model is validated against experimental data. Subsequently, application to Weldox 460E steel plates demonstrates excellent agreements in predicting critical thickness for transition of failure modes, ballistic limit, residual velocity, and the "plateau" phenomenon. Furthermore, the energy absorption mechanisms are discussed, and comparative analysis reveals distinct energy absorption mechanisms between Weldox 460E steel and 2024-T351 aluminium alloy plates.

1　Theoretical Model

For completeness, the theoretical model proposed by Yang *et al*.[22] is provided below. The perforation energy can be written as

$$E_{\mathrm{p}} = E_{\mathrm{im}} + E_{\mathrm{id}} + E_{\mathrm{sf}} + E_{\mathrm{gd}} \tag{1}$$

in which E_{p} is the perforation energy, comprising the energies absorbed by the initial inelastic impact (E_{im}), the local indentation (E_{id}), the local shear failure (E_{sf}), and the global deformations (E_{gd}).

E_{im} is determined by

$$E_{\mathrm{im}} = \frac{1}{2}\frac{m}{M+m}Mv_0^2 \tag{2}$$

in which v_0 is the impact velocity; M is the projectile mass; m is the plug mass, which can be written approximately as $m = \pi a^2 H\rho_{\mathrm{t}}$, with ρ_{t} being the plate density, a the radius of projectile, and H the plate thickness.

E_{id} is determined by

$$E_{\mathrm{id}} = \pi a^2 (1-\psi) H \int_0^{\varepsilon_{\mathrm{m}}} \left[K\varepsilon_X + \frac{2}{3}\sigma(\varepsilon_X) \right] \mathrm{d}\varepsilon_X \tag{3}$$

in which K is the bulk modulus of plate material; ψ is the ratio of the ultimate local indentation to the plate thickness; ε_{m} is the final compressive strain when the local indentation ends, $\varepsilon_{\mathrm{m}} = \ln[1/(1-\psi)]$; $\sigma(\varepsilon_X)$ denotes the yield stress when strain in the compression direction is ε_X. ε_X can be estimated by the following formula[17]

$$\sigma(\varepsilon)=\sqrt{3}\tau_0\left(\sqrt{3}\varepsilon\right)^n D_{\mathrm{m}}\exp\left[-\frac{\alpha\chi}{\rho_{\mathrm{t}}c_p}D_{\mathrm{m}}\frac{\tau_0}{n+1}\left(\sqrt{3}\varepsilon\right)^{n+1}\right] \tag{4}$$

in which τ_0, n and α are material constants; χ is the Taylor-Quinney coefficient, which is taken to be 0.9; c_p is the specific heat capacity of plate at constant pressure; D_{m} is the dynamic increase factor during perforation.

E_{sf} is determined by

$$E_{\mathrm{sf}}=2\delta\pi d(1-\psi)H\int_0^{\gamma_{\mathrm{f}}}\tau_0\gamma^n D_{\mathrm{m}}\exp\left(-\frac{\alpha\chi}{\rho_{\mathrm{t}}c_p}D_{\mathrm{m}}\frac{\tau_0}{n+1}\gamma^{n+1}\right)\mathrm{d}\gamma \tag{5}$$

in which γ is the shear strain; γ_{f} is the failure shear strain when shear plugging failure occurs; τ is the shear stress; δ is the half-width of shear band; d is the diameter of projectile.

E_{gd} is determined by

$$E_{\mathrm{gd}}=\frac{K_{\mathrm{m}}}{2}W_{\mathrm{o}}^2+F_{\mathrm{c}}W_{\mathrm{o}} \tag{6}$$

in which W_{o} is the transverse displacement at the periphery of impact area; K_{m} and F_{c} are the membrane stiffness and the static collapse load of plate, respectively, whose expressions can be found in Refs. [7, 22].

The dimensionless empirical equation describing the relationship between the global deformations and the impact velocity for the localized shear plugging with global deformations (Mode Ⅱ) is proposed by Yang *et al*.[22]

$$\frac{W_{\mathrm{o}}}{W_{\mathrm{os}}}=p_3\left\{1-\frac{2}{\pi}\arctan\left[p_1(\Phi-\Phi_{\mathrm{c}})\right]\right\}+(1-p_3)\exp\left[-p_2(\Phi-\Phi_{\mathrm{c}})\right] \tag{7}$$

in which p_1, p_2, and p_3 are empirical constants determined by curve fitting; W_{os} is the critical transverse displacement of plate when shear failure occurs in Wen-Jones model[7]

$$W_{\mathrm{os}}=\frac{\lambda}{2}d\left(0.41\frac{H}{d}+0.42\right)\ln\frac{R}{a}-\frac{1}{2\sqrt{3}}\left(\ln\frac{R}{a}+1+\frac{\sqrt{3}}{2}\right)H \tag{8}$$

in which $\lambda=\sigma_{\mathrm{u}}/\sigma_{\mathrm{y}}$, with σ_{u} and σ_{y} being the ultimate tensile strength and the yield strength of plate material, respectively; R is the radius of target plate. The dimensionless parameter Φ is expressed as

$$\Phi=\frac{\rho_{\mathrm{t}}v_{\mathrm{m}}^2}{\sigma_{\mathrm{y}}} \tag{9}$$

in which v_{m} is the common velocity of projectile and the impact area, determined by

$$Mv_0=(M+m)v_{\mathrm{m}} \tag{10}$$

Φ_{c} is the critical value of Φ at which the transition of failure modes occurs. For plates perforated in Mode Ⅰ (i. e., simple shear failure with global deformation), $W_{\mathrm{o}}/W_{\mathrm{os}}=1$.

Thus, the residual velocity can be obtained according to energy conservation

$$v_{\mathrm{r}}=\sqrt{\frac{Mv_0^2-2E_{\mathrm{p}}}{M+m}} \tag{11}$$

By letting $v_{\mathrm{r}}=0$ in Eq. (11), one obtains the equation of ballistic limit

$$v_{\mathrm{bl}}=\sqrt{\frac{2E_{\mathrm{p}}}{M}} \tag{12}$$

And according to Eq. (9), a critical impact velocity $v_{0\mathrm{c}}$ can be derived

$$v_{\mathrm{mc}}=\sqrt{\frac{\sigma_{\mathrm{y}}\Phi_{\mathrm{c}}}{\rho_{\mathrm{t}}}} \tag{13}$$

$$v_{0\mathrm{c}}=\frac{M+m}{M}v_{\mathrm{mc}}=\left(1+\frac{m}{M}\right)v_{\mathrm{mc}} \tag{14}$$

where v_{mc} is the critical velocity independent of plate geometry, and v_{0c} is the corresponding critical impact velocity when v_m equals to v_{mc}. Thus, the critical thickness H_c at which the transition of failure modes takes place can be determined as the thickness corresponding to the ballistic limit equals to v_{0c}.

2 Comparisons and Discussion

In this section, the model predictions are compared with available experimental data for the perforation of Weldox 460E steel plates by a flat-nosed projectile[18–21]. To further understand the perforation mechanisms, discussions on energy absorption are made, with a particular focus on the experimentally observed "plateau" phenomenon.

2.1 Comparisons with Experimental Data

Various parameters in the present model for Weldox 460E plates as studied by Børvik *et al.*[18–21] are listed in Table 1. It should be noted that the local indentation right after the initial inelastic impact is admittedly difficult to determine from experiments, but can be determined through numerical simulations[22]. Based on previous studies[13–14, 17], the local indentation ψ can be approximated in the following formula as a first-order approximation

$$\psi = \begin{cases} 0.065 & H/d \leqslant 0.5 \\ 0.07(H/d - 0.5) + 0.065 & H/d > 0.5 \end{cases} \tag{15}$$

Table 1　Parameters of the present model for Weldox 460E plates[17–21]

M/g	d/mm	R/mm	ρ_t/(kg·m^{-3})	K/GPa	c_p/(J·kg^{-1}·K^{-1})	τ_0/MPa
197	20	250	7850	196	452	540
n	D_m	α/K^{-1}	χ	γ_f	δ/μm	σ_y/MPa
0.25	2.1[23]	6.8×10^{-4}	0.9	3.12	100	490
σ_u/MPa	p_1	p_2	p_3	Φ_c		
580	1.83	35.73	0.2206	0.3080		

2.1.1 Relationship between Global Deformations and Impact Velocity

Fig.1 compares Eq. (7) with the experimental data of W_o/W_{os} versus $\Phi-\Phi_c$[21] for Weldox 460E steel plates perforated by a 20 mm diameter flat-nosed projectile. Fig.1 includes as well W_o/W_{os} versus $\Phi-\Phi_c$ for 2024-T351 aluminium plates from Ref. [22]. It is clear that good agreement is achieved between Eq. (7) and the experimental data. It should be noted here that the values of parameters p_1, p_2 and p_3 are maintained the same as in Ref. [22], which demonstrates the general applicability of Eq. (7).

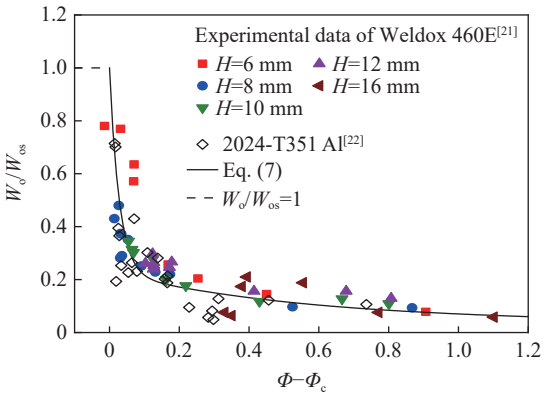

Fig. 1　Comparison of Eq. (7) with the experimental data of W_o/W_{os} versus $\Phi-\Phi_c$[21] for the Weldox 460E steel plates perforated by a flat-nosed projectile

2.1.2 Ballistic Limit and Residual Velocity

Fig.2 compares the theoretically predicted ballistic limits with the experimental data for Weldox 460E steel plates impacted by a 20 mm diameter flat-nosed projectile. It presents as well the numerically predicted ballistic limit for the 4 mm thick plate as reported by Børvik *et al.*[21] and the theoretically predicted ballistic limits given by Wen-Jones model[21] and Wen and Sun model[17]. By comparing the experimental data with the numerical result in Fig.2, it is evident that the present

model gives more consistent results than Wen-Jones model and Wen and Sun model. It is as well evident that the present model can predict the "plateau" phenomenon observed experimentally for plate thicknesses between 6 mm and 10 mm. It should be noted here that, for the 20 mm flat-ended projectile impacting Weldox 460E steel plates, the critical thickness H_c for the transition of failure modes is 5.54 mm, which agrees well with the experimental observation.

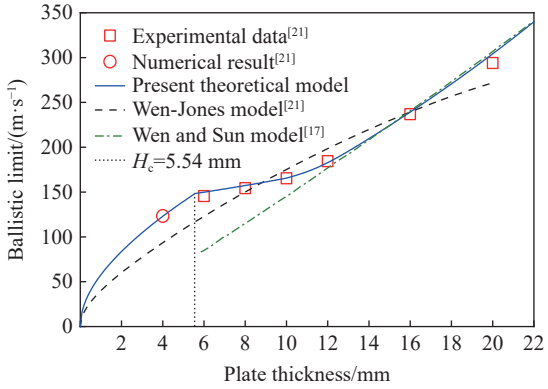

Fig. 2　Comparison between the theoretically predicted ballistic limits[17], the experimental data[21] and the numerical results[21] for the Weldox 460E plates impacted by a flat-nosed projectile

Fig.3 compares theoretically predicted residual velocities with experimental data for Weldox 460E plates with different thicknesses impacted by a 20 mm diameter flat-ended projectile[21]. It can be seen from Fig.3 that the predictions given by the present model are in good agreement with the experimental data for the plates with thicknesses less than 12 mm. For plate thicknesses of 16 mm and 20 mm, the difference between the theoretically predicted residual velocities and the test data increases as the impact velocity rises. It is reasonable to assume that plastic deformations of the projectiles become more severe at higher impact velocities and more energies are absorbed during this process[13–14]; however, this effect is not considered in the present model. This implies that the present model can give satisfactory predictions only when the projectile plastic deformation is negligible. Notably, the sharp increases in residual velocities close to the ballistic limits (termed "jump" by Børvik *et al.*[19, 21]) observed in the experiments are also well predicted by the present model. This is partly due to the fact that the global deformation drops suddenly (as shown in Fig.1), which leads to a considerable decline in energy absorption and a jump in residual velocity.

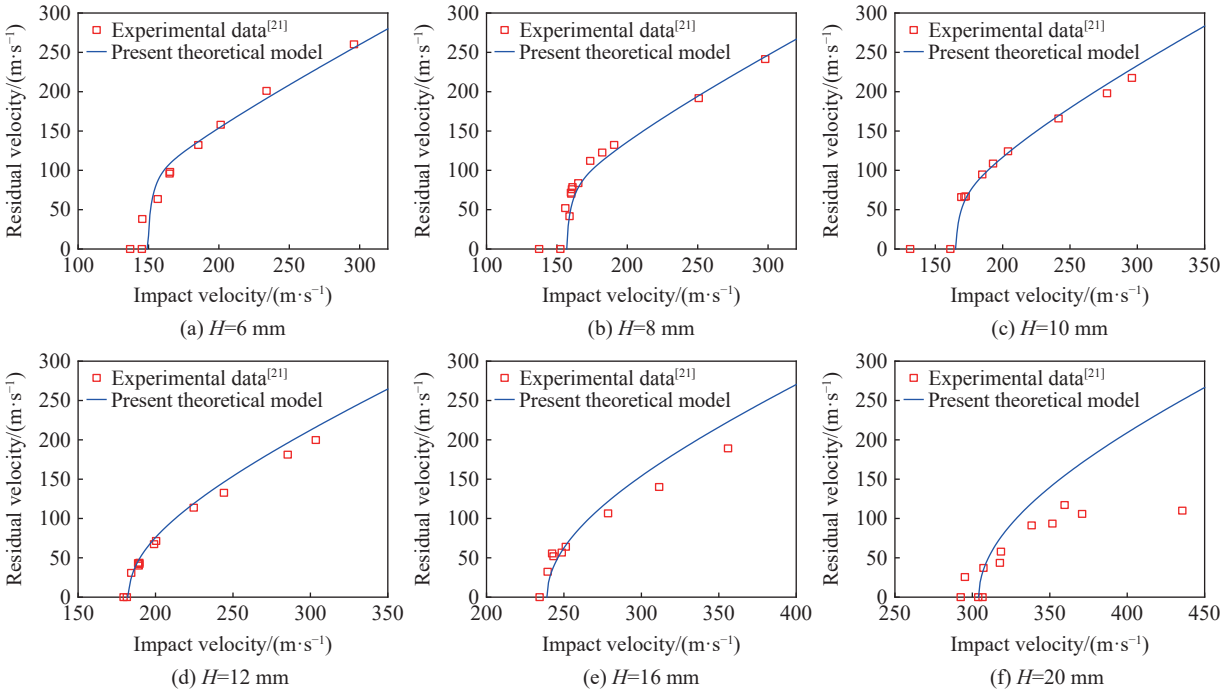

Fig. 3　Comparisons between the theoretically predicted residual velocities and the experimental data[21] for the Weldox 460E plates impacted by a 20 mm diameter flat-nosed projectile

2.2 Discussions on Energy Absorption

Fig.4 shows the relationships between the four parts of energy absorption of Weldox 460E steel plates and impact velocity of the 20 mm diameter flat-ended projectile. It is clear that the perforation energy first decreases and then increases with impact velocity, which is similar to the behavior of 2024-T351 plates[22]. Meanwhile, similar to the 2024-T351 plates, the impact energy of Weldox 460E steel plates increases with impact velocity, while the indentation and the shear failure energies remain unchanged within the impact velocity range examined.

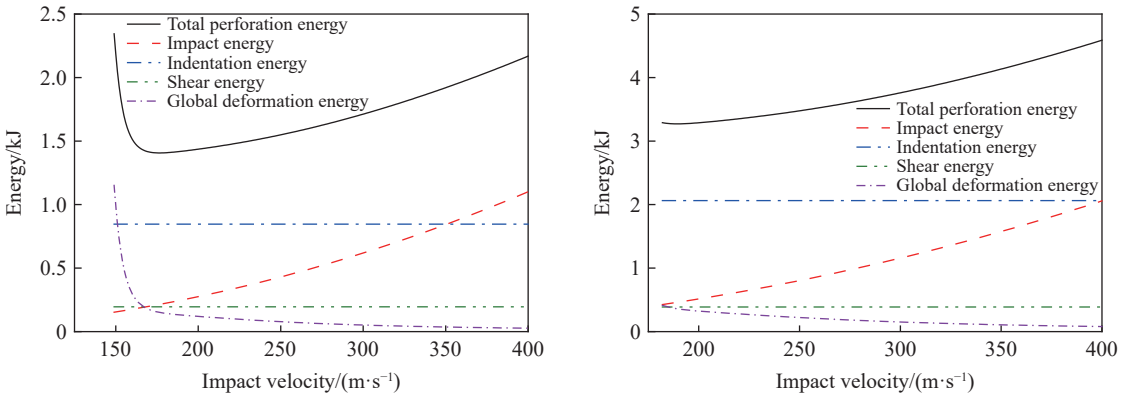

(a) H=6 mm　　(b) H=12 mm

Fig. 4　Relationships between the energy absorption of the Weldox 460E steel plates and the impact velocity of the 20 mm diameter flat-nosed projectile

Fig.5 shows the relationship between the ratios of these four parts (i. e., impact energy, indentation energy, shear energy and global deformation energy) to the total perforation energy with the impatct velocity. For the 6 mm thick Weldox 460E plate (Fig.5(a)), it is evident that the global deformation energy at the ballistic limit accounts for a large proportion (approximately 49%) of the total perforation energy. As the impact velocity increases, the ratio of global deformation energy decreases rapidly, leading to the “jump” phenomenon in residual velocity as the 2024-T351 plates[22]. The indentation energy accounts for a large proportion of the total perforation energy when the impact velocity is less than 350 m/s. For impact velocity greater than 350 m/s, the impact energy accounts for the largest proportion of total perforation energy. For the 12 mm thick Weldox 460E plate (Fig.5(b)), the proportion of the global deformation energy remains small even at ballistic limit, and it decreases further as the impact velocity increases. It should be mentioned here that the proportions of shear deformation energy in both plates are relatively small, which is about 10% for the impact velocity range examined. The proportion of indentation energy of Weldox 460E plates is much greater than that of 2024-T351 plates[22], which may be due to the high yield strength and the large local indentation of Weldox 460E steel.

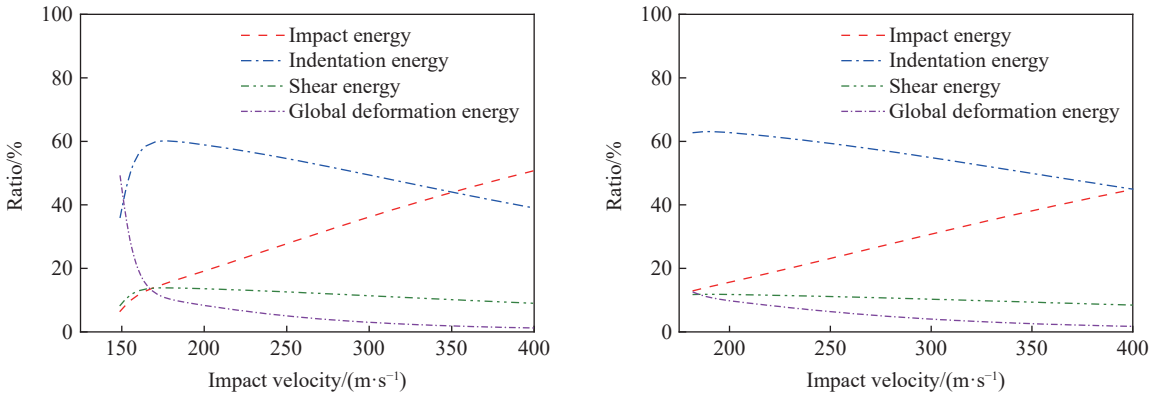

(a) H=6 mm　　(b) H=12 mm

Fig. 5　Relationship between the ratios of the four parts for the perforated Weldox 460E plates and the impact velocity

Fig.6 shows the variations of total perforation energy and its four parts at the ballistic limit with respect to thickness for the Weldox 460E plates impacted by the 20 mm diameter flat-nosed projectile. It can be seen from Fig.6 that the impact energy, indentation energy and shear energy at the ballistic limit increase with plate thickness. However, the global deformation energy first increases with plate thickness when $H \leqslant H_c$, and then decreases with thickness when $H>H_c$, which is significantly different from that of the 2024-T351 plates (for which the global deformation energy increases with thickness when $H>H_c$[22]). This is because the ballistic limit of Weldox 460E steel plates increases faster than that of 2024-T351 plates when $H>H_c$, resulting a faster decrease of the global deformation of Weldox 460E steel plates. Moreover, it can be seen from Fig.6 that the slope of indentation energy gets larger when $H>10$ mm, which corresponds to the change of the ψ-H relationship as described by Eq. (15).

Fig.7 shows the ratio variation of the four parts to the total perforation energy at the ballistic limit with plate thickness for Weldox 460E steel plates impacted by the 20 mm diameter flat-nosed projectile. It can be clearly seen from Fig.7 that the indentation energy at the ballistic limit accounts for a large proportion of the total perforation energy for Weldox 460E steel plates, particularly when $H>H_c$, which can be attributed to the high yield strength and the large local indentation of the Weldox 460E steel. Correspondingly, the global deformation energy accounts for only a small proportion of the total perforation energy at the ballistic limit for plates thicker than 12 mm. Therefore, it is reasonable to assume that global deformations for thick steel plates can be neglected as done in some existing theoretical models.

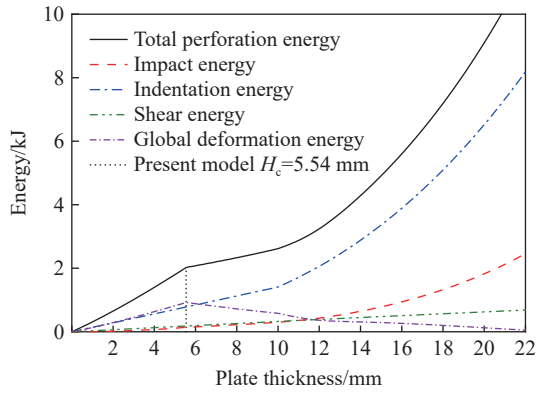

Fig. 6　Variations of the total perforation energy and its four parts at the ballistic limit with the thickness of the Weldox 460E plates impacted by the 20 mm diameter projectile

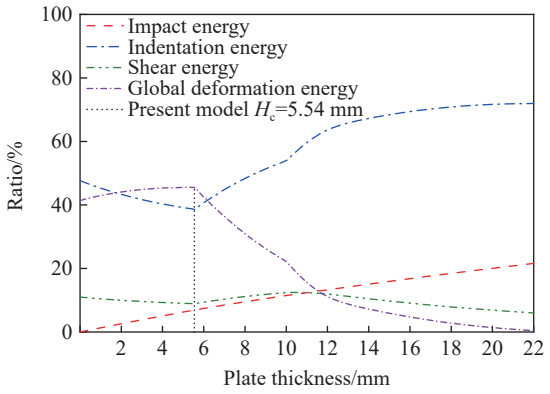

Fig. 7　Ratio variations of the four parts at the ballistic limit with the thickness of the Weldox 460E steel plates

3　Conclusions

In this study, the perforation of Weldox 460E steel plates impacted by a flat-nosed projectile has been investigated through a previously proposed theoretical model. The main conclusions are drawn as follows:

(1) The previously proposed empirical equation on the relationship between global deformation and impact velocity can effectively describe the experimental data of Weldox 460E steel plates, which lends further support to the accuracy and generality of the model.

(2) The predictions given by the model are in good agreement with the experimental and numerical results of Weldox 460E steel plates, including ballistic limit, residual velocity, the critical conditions for transition of failure modes, and the “plateau” phenomenon in the intermediate plate thickness range examined.

(3) The energy absorption mechanisms of Weldox 460E steel plates are analyzed and discussed using the theoretical model. Compared with 2024-T351 aluminium plates, the indentation energy of Weldox 460E plates

takes more significant proportion of the total perforation energy, which can be attributed to the high yield strength and large local indentation of Weldox 460E steel.

(4) For Weldox 460E steel plates, the energies absorbed by indentation and global deformations at ballistic limit are nearly equal for thin plates which are failed by Mode Ⅰ (simple shear failure with global deformations). For thick plates failed by Mode Ⅱ (localized shear plugging), the indentation energy increases significantly with plate thickness, whereas the global deformation energy decreases sharply.

References:

[1] CORBETT G G, REID S R, JOHNSON W. Impact loading of plates and shells by free-flying projectiles: a review [J]. International Journal of Impact Engineering, 1996, 18(2): 141–230.

[2] BEN-DOR G, DUBINSKY A, ELPERIN T. Ballistic impact: recent advances in analytical modeling of plate penetration dynamics: a review [J]. Applied Mechanics Reviews, 2005, 58(6): 355–371.

[3] ROSENBERG Z, DEKEL E. Terminal ballistics [M]. 3rd ed. Cham: Springer, 2020.

[4] SHADBOLT P J, CORRAN R S J, RUIZ C. A comparison of plate perforation models in the sub-ordnance impact velocity range [J]. International Journal of Impact Engineering, 1983, 1(1): 23–49.

[5] WOODWARD R L. A structural model for thin plate perforation by normal impact of blunt projectiles [J]. International Journal of Impact Engineering, 1987, 6(2): 129–140.

[6] LIU D Q, STRONGE W J. Perforation of rigid-plastic plate by blunt missile [J]. International Journal of Impact Engineering, 1995, 16(5/6): 739–758.

[7] WEN H M, JONES N. Low-velocity perforation of punch-impact-loaded metal plates [J]. Journal of Pressure Vessel Technology, 1996, 118(2): 181–187.

[8] 徐伟, 侯海量, 朱锡, 等. 平头弹低速冲击下薄钢板的穿甲破坏机理研究 [J]. 兵工学报, 2018, 39(5): 883–892.
XU W, HOU H L, ZHU X, et al. Investigation on the damage mechanism of blunt projectile against thin plate [J]. Acta Armamentarii, 2018, 39(5): 883–892.

[9] RECHT R F, IPSON T W. Ballistic perforation dynamics [J]. Journal of Applied Mechanics, 1963, 30(3): 384–390.

[10] WOODWARD R L, DE MORTON M E. Penetration of targets by flat-ended projectiles [J]. International Journal of Mechanical Sciences, 1976, 18(3): 119–127.

[11] RAVID M, BODNER S R. Dynamic perforation of viscoplastic plates by rigid projectiles [J]. International Journal of Engineering Science, 1983, 21(6): 577–591.

[12] CHEN X W, LI Q M. Shear plugging and perforation of ductile circular plates struck by a blunt projectile [J]. International Journal of Impact Engineering, 2003, 28(5): 513–536.

[13] LU Z C, HE Y, WEN H M, et al. A plastic wave model for the perforation of a finite metal plate struck by a flat-ended projectile [J]. International Journal of Impact Engineering, 2023, 173: 104466.

[14] CAO S, FAN J T. Numerical model for penetration process of a deformable projectile into ductile metallic target plate considering the interaction of projectile and target [J]. International Journal of Impact Engineering, 2025, 195: 105107.

[15] BAI Y L, JOHNSON W. Plugging: physical understanding and energy absorption [J]. Metals Technology, 1982, 9(1): 182–190.

[16] CHEN X W, LI Q M, FAN S C. Initiation of adiabatic shear failure in a clamped circular plate struck by a blunt projectile [J]. International Journal of Impact Engineering, 2005, 31(7): 877–893.

[17] WEN H M, SUN W H. Transition of plugging failure modes for ductile metal plates under impact by flat-nosed projectiles [J]. Mechanics Based Design of Structures and Machines, 2010, 38(1): 86–104.

[18] BØRVIK T, LANGSETH M, HOPPERSTAD O S, et al. Ballistic penetration of steel plates [J]. International Journal of Impact Engineering, 1999, 22(9/10): 855–886.

[19] BØRVIK T, LEINUM J R, SOLBERG J K, et al. Observations on shear plug formation in Weldox 460E steel plates impacted by blunt-nosed projectiles [J]. International Journal of Impact Engineering, 2001, 25(6): 553–572.

[20] BØRVIK T, HOPPERSTAD O S, BERSTAD T, et al. A computational model of viscoplasticity and ductile damage for impact and penetration [J]. European Journal of Mechanics A: Solids, 2001, 20(5): 685–712.

[21] BØRVIK T, HOPPERSTAD O S, LANGSETH M, et al. Effect of target thickness in blunt projectile penetration of Weldox 460E steel plates [J]. International Journal of Impact Engineering, 2003, 28(4): 413–464.

[22] YANG L F, WEN H M. A numerical and theoretical study on the perforation of aluminum plates struck by flat-nosed projectiles [J/OL]. Acta Mechanica Solida Sinica [2024-10-17]. https://link.springer.com/article/10.1007/s10338-024-00557-6. DOI: 10.1007/s10338-024-00557-6.

[23] 王子豪, 郑航, 文鹤鸣. 金属材料在极高应变率下的力学性能测试 [J]. 高压物理学报, 2020, 34(2): 024102.
WANG Z H, ZHENG H, WEN H M. Determination of the mechanical properties of metals at very high strain rates [J]. Chinese Journal of High Pressure Physics, 2020, 34(2): 024102.

简论钢板在平头弹撞击下的穿透

杨岚夫, 文鹤鸣

（中国科学技术大学近代力学系, 中国科学院材料力学行为和设计重点实验室, 安徽 合肥　230027）

摘要: 利用先前提出的统一框架内平头弹穿透有限金属靶板的理论模型, 对平头弹撞击下 Weldox 460E 钢板的穿透问题进行了研究。该模型包含一个无量纲半经验方程, 考虑了整体变形吸能随撞击速度的变化, 由此讨论了 Weldox 460E 钢板的能量吸收机理, 解释了“平台”现象（随着板厚的增大, 弹道极限的提高有限）, 并将 Weldox 460E 钢板结果与先前研究的 2024-T351 铝板结果进行了对比。结果表明: 模型预测的 Weldox 460E 钢板在平头弹撞击下的整体变形与撞击速度之间的关系、弹道极限、残余速度以及破坏模式临界转化条件等均与实验结果吻合得很好; 模型也能很好地预测中厚板范围内的“平台”现象。与 2024-T351 铝板相比, 被平头弹贯穿的 Weldox 460E 钢板的压入吸能在总吸能中的占比明显更大, 这是两种靶板材料的不同特性所导致的。

关键词: 理论模型; 平头弹; 钢板; 穿透; 弹道极限; 残余速度

中图分类号: O385; O521.9　　**文献标志码:** A